4D STEM: High efficiency phase contrast imaging using a fast pixelated detector

2015 J. Phys.: Conf. Ser. 644 012032

(http://iopscience.iop.org/1742-6596/644/1/012032)

4D STEM: High efficiency phase contrast imaging using a fast pixelated detector

H Yang[1], L Jones[1], H Ryll[2], M Simson[3], H Soltau[3], Y Kondo[4], R Sagawa[4], H Banba[4], I Maclaren[5], and P D Nellist[1]

1. Department of Materials, University of Oxford, Parks Rd, Oxford UK
2. PNSensor GmbH, Otto-Hahn-Ring 6, 81739 München, Germany
3. PNDetector GmbH, Sckellstraße 3, 81667 München, Germany
4. JEOL Ltd.,3-1-2 Musashino Akishima Tokyo 196-8558 Japan
5. University of Glasgow, Glasgow G12 8QQ, UK

hao.yang@materials.ox.ac.uk

Abstract. Phase contrast imaging is widely used for imaging beam sensitive and weak phase objects in electron microscopy. In this work we demonstrate the achievement of high efficient phase contrast imaging in STEM using the pnCCD, a fast direct electron pixelated detector, which records the diffraction patterns at every probe position with a speed of 1000 to 4000 frames per second, forming a 4D STEM dataset simultaneously with the incoherent Z-contrast imaging. Ptychographic phase reconstruction has been applied and the obtained complex transmission function reveals the phase of the specimen. The results using GaN and Ti, Nd-doped $BiFeO_3$ show that this imaging mode is especially powerful for imaging light elements in the presence of much heavier elements.

1. Introduction

Phase contrast imaging using elastic electron scattering has been shown to provide the highest dose efficiency for imaging weak phase objects for a given amount of radiation damage, as compared to inelastic electron scattering, as well as to X-ray and neutron scattering[1]. Therefore phase contrast imaging in the conventional transmission electron microscope (CTEM) continues to play a critical role in many biological studies.

There has been growing interests in developing phase contrast imaging modes in the scanning transmission electron microscopy (STEM), because of its flexibility in allowing innovations in detector geometry without modifying the main optics of the electron column and the ability to simultaneously record incoherent and analytical signals. For example, annular bright field (ABF) [2-4] and differential phase contrast (DPC) [5,6] have been demonstrated as being sensitive to light elements and electrical/magnetic fields. However, recent studies have shown that bright field (BF) and ABF are not efficient for imaging weak phase objects because interferences between diffracted and direct beams carrying positive and negative phases cancel under zero aberrations using any centrosymmetric detector geometry[7,8]. The greatest signal is obtained if the regions of constructive and destructive interferences are covered by separate detectors[9].

This can be achieved by using fast pixelated detectors that record the CBED pattern at every probe position forming a 4-dimensional dataset. The phase can be extracted through post-processing using a method called ptychography[10], which makes use of the redundancy in the 4D dataset. Various

ptychographic reconstruction methods have been developed in both electron and X-ray microscopy to retrieve the phase through either iterative[11,12] or direct inversion approaches[13–15]. Partially due to the practical difficulties in recording the 4D dataset due to limited camera speed, the most common practice in literature was to use a defocused probe[16] to increase the illuminated area, thus reducing the number of probe positions needed to ensure overlapping between the neighboring probe illuminating areas in order to solve the ambiguity in phase. However, with recent advances in detector technology, which have massively improved the camera speed, 4D STEM can be recorded with a large number of probe positions and a sub-Ångström focused probe that makes full use of the aberration corrector. In this way incoherent Z-contrast imaging with a high angle annular dark field (HAADF) detector and even analytical signals can be obtained simultaneously with the diffraction patterns that yield the reconstructed phase.

Here in this work we show that making use of a fast pixelated detector installed on an aberration corrected STEM, 4D datasets recorded using an aberration corrected electron probe combined with ptychography offers a new phase contrast imaging mode in STEM and opens opportunities for imaging weak phase objects and detecting light elements with high efficiency.

2. Experimental methods

The experiments were performed using a pnCCD (S)TEM camera, a direct electron radiation-hard pixelated detector from PNDetector GmbH, mounted on a JEOL ARM200CF aberration corrected microscope. This camera delivers a readout speed of 1000 full frames per second (fps) routinely[17], and up to 20,000 fps through binning/windowing. For a typical STEM scanning consisting of 256x256 probe positions, a 4D dataset consisting of 264x264 pixel diffraction patterns for each probe position can be recorded in less than 70 seconds. Figure 1 shows single frames of the convergent beam electron diffraction (CBED) patterns recorded at different detector binning levels and frame times, and single electron events can be seen clearly in the dark field regions. Synthetic BF, ABF and DPC images can also be obtained from the diffraction patterns, with the full flexibility to tune the collection angles in ABF and partition direction of the DPC segments. Z-contrast HAADF images were usually recorded simultaneously using an annular dark field (ADF) detector.

3. Results and discussion

The ptychographic reconstruction approach applied to the 4D datasets used in this work follows Rodenburg *et al*.[14] The reader is referred to the previous works[14,7] for the details of the reconstruction procedure. By taking the Fourier transform of the 4D dataset with respect to probe positions, interferences between the direct beam and the diffracted beams of specific diffraction angles can be isolated in the detector plane, and the phase information can be extracted from the regions of disc-overlapping between the direct and diffracted beams. An experimental example of the overlapping discs from an Au nanoparticle sample at a single spatial frequency is shown in Figure 2. The two diffracted discs overlap with the direct beam to form single overlap regions, and all three discs overlap to form a double overlap region in the middle. Under the weak-phase approximation, the two sides of the single overlap regions are "flat" and π out of phase, and the phases in the double overlap completely cancel. Therefore the complex quantity can be integrated from one side of the disc-overlapping regions at each spatial frequency, and the phase can be reconstructed by calculating the inverse Fourier transform of the integrated phase with respect to probe positions.

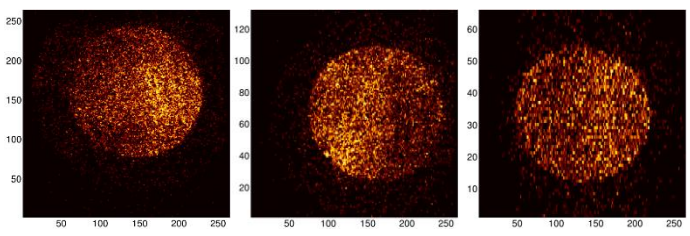

Figure 1. Examples of individual frames of CBED patterns consisting of primarily the bright field disk with three different binning and speed: (a) 1000 fps without binning, (b) 2000fps with 2-fold binning and (c) 4000 fps with 4-fold binning.

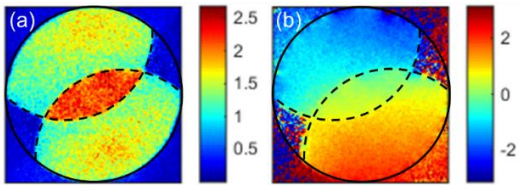

Figure 2. An experiment example of the (a) modulus and (b) phase of the interference between the direct beam (solid circle) and two diffracted beams (dashed circles) in the detector plane, showing single and double disc-overlapping regions. The colour-bar in (b) is in unit of radian.

Experiments have been applied to an Au nanoparticle on a carbon support. The simultaneous HAADF, ABF, and the modulus and phase of the phase reconstruction from an Au nanoparticle with five-fold twinning have been obtained and shown in Figure 3a-d). The ptychographic phase reconstruction shows good contrast in both the modulus and phase across thick and thin regions of the nanoparticle. In comparison, the synthetic ABF image shows decreasing contrast towards the edge of the Au nanoparticle, suggesting that ABF, as a nonlinear imaging mode, is not very efficient when the specimen is very thin, and relies on phase shift from lens aberrations and defocus to form the image contrast for thin specimens that obey a weak phase object approximation[3]. The improved contrast in ABF with increasing thickness can be ascribed to the multiple scattering channelling processes[18]. Furthermore, the ptychographic reconstruction shows a clearer texture in the carbon support region than in the ABF, indicating its high sensitivity to weakly scattered objects. Moreover, based on the reconstructed phase in unit of radians, the projected potential can be directly calculated using the interaction constant, and the atomic electric field could also be derived by calculating the first derivative of the potential[19].

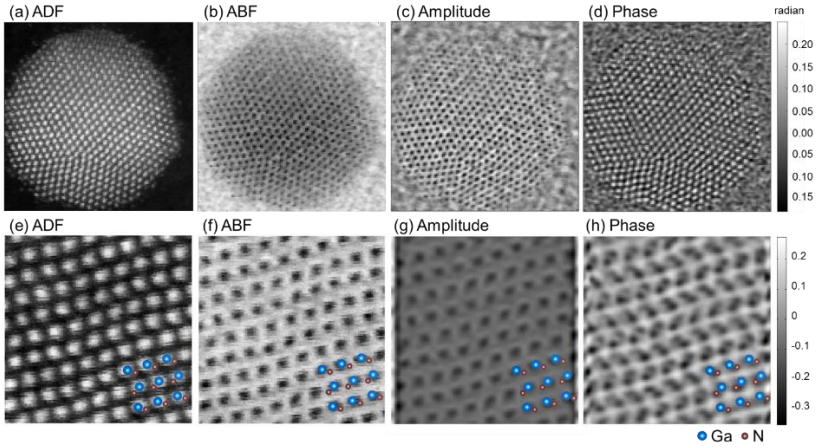

Figure 3. Simultaneous ADF, synthetic ABF, and the reconstructed amplitude and phase of (a-d) an Au nanoparticle and (e-h) GaN bulk lattice viewed along $[2\bar{1}\bar{1}0]$. The probe forming aperture for cases is about 14.4 mrad, and the synthetic ABF has a collection angle of 7.2-14.4 mrad.

The results of ptychographic phase reconstruction of GaN viewed along $[2\bar{1}\bar{1}0]$ demonstrates the sensitivity to imaging light elements, as shown in Figure 3e-h. N columns are not clearly visible in the ABF image (Figure 3f) using a 14mrad semi-angle convergence aperture with a theoretical resolution of about 0.9 Å. In contrast, the Ga-N dumbbells are clearly resolved in the reconstructed complex transmission function. The N columns give their clearest contrast in the phase image (Figure 3h). And in the modulus the major peak corresponds to the heavy Ga column because the modulus contrast comes primarily from absorption (Figure 3g).

Ptychographic phase reconstruction has also been applied to charged antiphase domain boundaries in Nd, Ti doped $BiFeO_3$[20,21]. Oxygen columns are clearly resolved in both the bulk and the boundary (Figure 4), which are not seen in the HAADF image, and are barely visible in the ABF image. The Fe/Ti columns are strong features in the reconstructed phase, as might be expected. On the other hand, the Bi columns show broad but rather low intensity diffused features in the reconstructed phase. This is almost certainly caused by strong phase shifts on these high-Z columns, leading in the direction of a contrast inversion, as is commonly observed in phase contrast high resolution TEM (HRTEM).

Nevertheless, the region is still thin enough that all atoms are imaged in positive contrast using this ptychographic reconstruction method under the weak phase approximation.

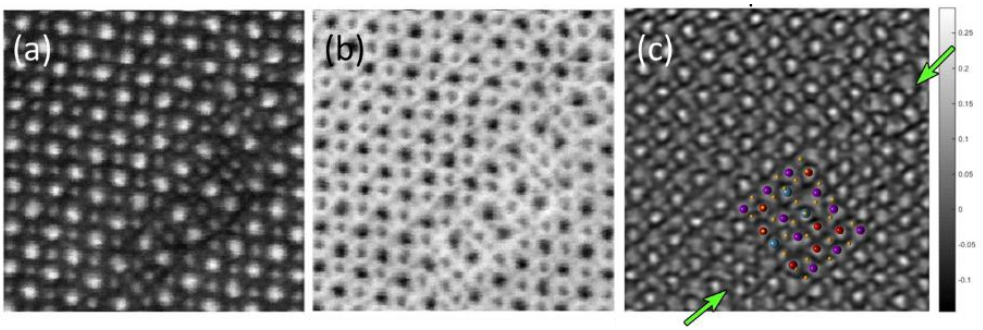

Figure 4. HAADF, synthetic ABF and the reconstructed phase of an antiphase boundary in Ti, Nd doped $BiFeO_3$. It should be noted that the oxygen positions which are invisible in the HAADF image appear in the phase image as small yellow peaks. The larger red peaks are B-site Fe columns, the blue peaks are B-site Ti columns, and the bright purple peaks are A-site (Bi/Nd) columns.

4. Conclusion

In conclusion we have shown that using a pnCCD pixelated detector, a highly efficient phase contrast imaging mode may be achieved by applying ptychography to the 4D STEM datasets, which opens various fields of applications for imaging weak phase objects and light elements, which are complementary to the well-established incoherent Z-contrast imaging in STEM.

The authors acknowledge funding from the EPSRC (grant numbers EP/K032518/1, EP/K040375/1 EP/M009963/1 and EP/M010708/1) and the EU FP7 Grant Agreement 312483 (ESTEEM2).

References

[1] Henderson, R. *Q. Rev. Biophys.* **28,** 171–193 (1995)
[2] Rose, H. *Ultramicroscopy* **2,** 251–267 (1976)
[3] Ishikawa, R. *et al*. *Nat. Mater.* **10,** 278–81 (2011)
[4] Okunishi, E. *et al. Microsc. Microanal*. **15**, 164-165 (2009)
[5] Dekkers, N. H. & Lang, H. D. *Optik.* **41,** 452–456 (1974)
[6] Shibata, N. *et al. Nat. Phys.* **8,** 611–615 (2012)
[7] Pennycook, T. J. *et al. Ultramicroscopy* **151,** 160–167 (2015)
[8] Yang, H. *et al*. *Ultramicroscopy* **151,** 232–239 (2015)
[9] Rose, H. *Ultramicroscopy* **2,** 251–67 (1977)
[10] Hoppe, W. *Acta Crystallogr. A* **25**, 495-501 (1969)
[11] Maiden, A. M.*et al. Ultramicroscopy* **109,** 1256–62 (2009)
[12] Thibault, P. *et al. Science* **321,** 379–82 (2008)
[13] Rodenburg, J. M. *et al*. *Philo. Trans.Roy. Soc. A* **339,** 521–553 (1992)
[14] Rodenburg, J. M. *et al*. *Ultramicroscopy* **48,** 304–314 (1993)
[15] D'Alfonso, A. J. *et al. Phys. Rev. B*. **89,** 064101 (2014)
[16] Humphry, M. J. *et al*. *Nat. Commun.* **3,** 730 (2012)
[17] Ryll, H. *et al. Microsc. Microanal.* **20,** 1122–1123 (2014)
[18] Findlay, S. *et al*. *Ultramicroscopy* **110**, 903-923 (2010)
[19] Cowley, J. M. *Electron Diffraction Techniques. Vol. 1*. Oxford University Press (1992)
[20] MacLaren, I. *et al. APL Mater*. **1,** 021102 (2013)
[21] MacLaren, I. *et al. APL Mater*. **2,** 066106 (2014)